THERMAL MODELLING OF THE IN-SITU CONSOLIDATION OF AUTOMATED FIBER PLACEMENT OF THERMOPLASTIC COMPOSITES

Christopher J. Stelter[1], Thammaia Sreekantamurthy[2], Tyler B. Hudson[1], Brian W. Grimsley[1]

[1]NASA Langley Research Center, Hampton, VA 23681
[2]Analytical Mechanics Associates, Inc., Hampton, VA 23681

ABSTRACT

NASA is developing carbon fiber reinforced thermoplastic composites processing methods under the Hi-rate Composites Aircraft Manufacturing (HiCAM) project. The in-situ consolidation automated fiber placement (AFP) of thermoplastics (ICAT) process has high potential to increase manufacturing throughput and lower costs as it combines the repeatability and fast lay down rates of AFP with the thermoformability of thermoplastic materials to achieve part consolidation out of the autoclave. Physics-based process models are employed in the ICAT process development to understand, fundamentally, the thermal response of the carbon fiber (CF)/polyaryletherketone (PAEK) material during the rapid heating and cooling associated with laser-assisted AFP. A one-dimensional (1-D) closed-form model was developed capable of predicting the temperature profile through-the-thickness of the tape material. In addition, a two-dimensional (2-D) model was developed to predict the heat transfer through-the-thickness and in the laydown *x*-direction of the AFP head motion. The solution of the Fourier heat-transfer equations in the 2-D model is approximated using the explicit finite difference numerical method. The temperature profile during placement of PAEK slit-tape materials at various laser target temperatures and placement speeds were measured during ICAT process development trials at Electroimpact®, Inc. [††] and the resulting experimental data is compared with the predictions of the 1-D and 2-D models.

Keywords: Thermoplastics, Composites, Automated Fiber Placement, Process Modeling
Corresponding author: Christopher J. Stelter; christopher.j.stelter@nasa.gov

1. INTRODUCTION

The NASA Hi-rate Composites Aircraft Manufacturing (HiCAM) project is developing advanced composites manufacturing technology for aircraft to enable faster production of composite airframes and components while minimizing both labor and equipment capital costs [1]. One of the initiatives under HiCAM investigates thermoplastic composites to enable the project goals, specifically looking toward in-situ consolidation of the composite, avoiding the need for expensive and cycle-time-limiting autoclave or oven post-processing.

Autoclaves are capital-intensive and require extensive facility support, even compared to large composite processing ovens. In contrast to thermoset composites, thermoplastics have the potential to reduce this capital cost as they are melt-processed instead of cured and can, in principle, be

[††]Specific vendor and manufacturer names are explicitly mentioned only to accurately describe the hardware used in this study. The use of vendor and manufacturer names does not imply an endorsement by the U.S. Government, nor does it imply that the specified equipment is the best available.
SAMPE Conference Proceedings. Long Beach, CA May 20-23, 2024. Society for the Advancement of Material and Process Engineering – North America.

consolidated during the layup process instead of during a post-process. Attempting high-rate in-situ consolidation means speeding up the layup process significantly but allowing sufficient time for welding of the incoming tape ply to the substrate ply. The welding process requires that the incoming tape establish intimate contact with the previously laid tape, or substrate. Once in contact, polymer molecular chain reptation must occur for the thermoplastic weld to develop inter-ply design strength. Degree of intimate contact increases as a function of elapsed time, pressure, and temperature. Reptation increases as a function of elapsed time and temperature. In both cases, the material generally needs to be above the crystalline melt temperature for bond strength to increase. Too high of a temperature can also damage the thermoplastic polymer, causing breakdown of the polymer chains through chain scission or even decomposition. For these reasons, a careful understanding of the temperature of the incoming tape and substrate during the layup process is necessary for improving the processing of the material, ensuring both successful layup at appropriate speed and the development of required bond strength [2].

Investigating ICAT in the HiCAM project required initial estimates of thermal profile boundaries to assess the feasibility of the in-situ consolidation and to plan for process design of experiments at the Electroimpact® AFP vendor facility. A review of the previous research on laser assisted thermoplastic AFP indicated that the thermal responses in the in-situ consolidation region are affected by a variety of factors such as laser beam optics, laser power distributions on the consolidating tapes, thermoplastic material characteristics such as melting and degradation temperatures, and the medium of heat transfer such as conduction, convection, and radiation [3, 4]. Laser light energy is absorbed (dependent on wavelength, angle of incidence, and reflections) into the composite material as heat [3, 4]. Several thermal analysis approaches in the past for the AFP process, ranging from a simple 1-D steady state solution, a 1-D transient solution, to 2-D and 3-D transient solutions have been developed [5, 6]. Heat transfer analysis of the laser heated thermoplastic tape was performed to provide a quick estimate of the temperature range expected during the ICAT process. This paper addresses heat transfer analysis using 1-D and 2-D models to predict temperature responses critical to the success of ICAT. Predicted temperature response results are compared with NASA ICAT experiments performed at the Electroimpact® facility [7].

2. THERMAL ANALYSIS METHODOLOGY

2.1 One-dimensional Thermal Model Methodology

Heat transfer modeling of the ICAT process in its simplest form is based on the observation that the rate of heat flow in the fiber direction is much smaller in magnitude relative to the mass transport associated with the material [2]. Also, the thermal problem in tape placement can be simplified based on the heat conduction path, whether heat migrates quickly to the back side of the tape of finite thickness or where this is ruled out in substrate layers of tape laid on the tool surface, in which case the thermal problem can be idealized as that of a semi-infinite thickness material [6]. This assumption enables the use of closed-form thermal analysis solutions to predict the tape surface temperature [4].

The 1-D thermal model described here simplifies the many complex thermal phenomena of this process to the point where tractable analytical solutions exist while retaining the most significant elements. Simplified analysis was sought noting that the predominant mode of heat transfer is conduction, although other modes such as convection and radiation are present to a lesser extent

in ICAT. The generalized heat conduction equation satisfies conservation of energy. A simple 1-D thermal analysis, sufficiently representative of the laser heat transfer process of the tape in the vicinity of the nip point of the consolidation roller (Figure 1), is considered here. With no internal heat generation and the assumption of constant thermal conductivity, the heat equation can be written in the 1-D form as in Equation (1).

$$\frac{\partial T}{\partial \tau} = \alpha \frac{\partial^2 T}{\partial y^2}, \qquad \tau = \frac{x}{V} \tag{1}$$

In Equation (1), α is the thermal diffusivity as a function of material characteristics along the y direction such as thermal conductivity, density, and specific heat; T is the temperature through the thickness direction, y; V is the roller head speed, and τ and x are the time normalized with speed and location along the tape surface, respectively. The boundary conditions on the problem include the heat flux on the tape top surface, and an insulation boundary on the far side of the consolidated layers of the substrate tape.

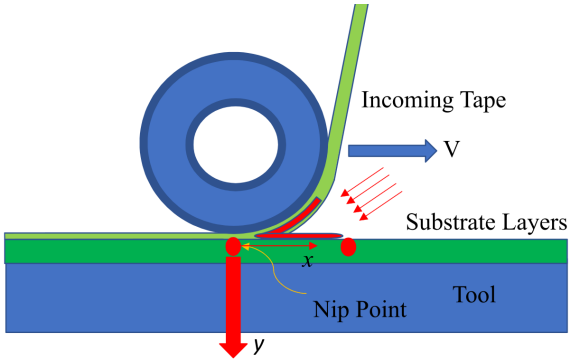

Figure 1: Schematic of laser heated AFP.

The substrate tape layers built up on the tool surface can be considered thick compared to the thin thermoplastic incoming tape that is placed as a new substrate layer. Therefore, the pre-heated substrate layers can be idealized as a solid slab for seeking a simple solution. If a sudden laser heat is imposed on this surface, then transient 1-D conduction will occur in the solid. Analytical solutions are readily available for transient response of the semi-infinite solid. Therefore, a closed form solution [Equation (2)] can be readily obtained for the temperature on the tape surface as well as the temperature through the thickness [8] of the substrate for any time duration of laser exposure producing a heat flux on the tape surface. The heat flux on the tape surface at the roller nip point can be calculated [4] for a known incident angle of the laser beam on the substrate.

$$T(y,t) = T_i + \frac{2q_0''\sqrt{\alpha t}}{k} i\,\mathrm{erfc}\left(\frac{y}{2\sqrt{\alpha t}}\right) \tag{2}$$

In Equation (2), T_i is the initial temperature of the material; T is the final temperature at depth y and time t; k and α are the thermal conductivity and diffusivity of the material, respectively; i erfc is the complementary error function; and the laser heat flux q_0'' is a function of the laser power and absorptance of the material.

The heat flux is a function of the optical geometry of the laser beam (of width w and depth h) directed toward the nip point at an incident angle β. The elliptical laser spot is split to form spots which are incident on both the substrate and incoming tapes with projected spot lengths of h_1' and h_2' (or arc length of s), respectively, as shown in Figure 2. There are two possibilities in the heating of the thin incoming tape (Figure 2). In Case A (solid green line), the incoming tape is wrapped around the roller (of radius r) with a large thermal mass, therefore the semi-infinite solid approach would be sufficiently representative of the heat transfer problem and hence followed here. On the other hand, if the thin incoming tape is pre-exposed as in Case B (dotted green line), before getting wrapped around roller, then the finite thickness solution [6, 9] (Equation (3)) would be more appropriate instead of the semi-infinite solution, as heat quickly reaches the back surface of the tape that is not in intimate contact with the roller surface, where Fo is the Fourier number.

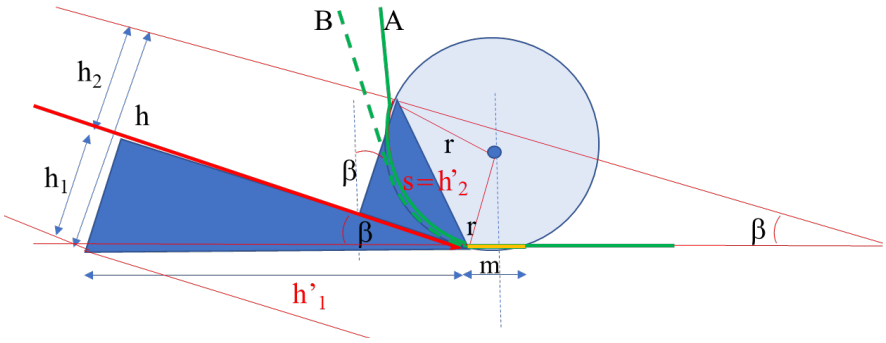

Figure 2: Schematic of laser beam geometry and spot size.

$$T(y,t) = T_0 + \frac{q_0'' L}{k}\left[F_0 + \frac{\left(\frac{y}{L}\right)^2}{2} - \frac{y}{L} + \frac{1}{3} - \frac{2}{\pi^2}\sum_{n=1}^{\infty}\frac{\cos\{n\pi(\frac{y}{L})^2\}}{n^2}e^{-(n\pi)^2 F_0}\right] \quad (3)$$

As the incoming tape section goes past the roller nip point, the portion of roller footprint (m), and the tape beyond the rear of the roller would no longer be under the laser spot, and the loss of heat flux results in immediate cooling of the tape. The temperature sustained in the tape after a fraction of exposure time just before undergoing consolidation at the nip point is critical to the formation of autohesion (welding) and co-fusion of the incoming tape to the substrate layer of tape. The cooling response of a tape is readily obtained from a simplified solution [6] of the heat transfer differential equation for conduction, Equation (4).

$$T(y,t,t_p) = T_0 + \frac{2q_0''}{k}\left[i\,\mathrm{erfc}\left\{\left(\frac{y}{\sqrt{4\alpha t}}\right)\right\}\sqrt{\alpha t} - i\,\mathrm{erfc}\left\{\left(\frac{y}{\sqrt{4\alpha(t-t_p)}}\right)\right\}\sqrt{\alpha(t-t_p)}\right] \quad (4)$$

In Equation (4), t_p is the heating time, t_c is cooling time and t is the total time. The cooling time t_c is obtained by subtracting the heating time t_p from total time t, $t_c = t - t_p$.

The heat transfer that occurs when the heated incoming tape is in contact with the substrate can be idealized as two semi-infinite solids (subscript 1 and 2) in contact at the tape interface with two different initial temperatures $T_{1,i}$ and $T_{2,i}$ [10]. This results in heat flow between the two bodies at

their contact surfaces. The transient thermal response due to the heat flow between two bodies is determined according to [6], leading to an equilibrium temperature determined by Equation (5).

$$T_s = \frac{m_1 T_{1,i} + m_2 T_{2,i}}{m_1 + m_2} \tag{5}$$

In Equation (5), the quantity $m = \sqrt{k\rho c}$ is a weighting factor, where *k,* ρ and *c* are thermal conductivity, mass density and specific heat of the material, respectively. In a simpler situation where $m_1 = m_2$, the resulting surface temperature T_s is the average temperature of the two surfaces.

The closed-form solution of the 1-D thermal analysis was implemented in a Microsoft® EXCEL® spread sheet, to provide a physics-based estimate of the heating response through the thickness. The thermal analysis is performed with laser heating parameters such as laser power, laser spot split ratio, absorptance, and angle of incidence (AoI) as inputs to calculate the heating and cooling response of the substrate and incoming tapes, and resultant temperature after tapes come into contact at the nip point.

2.2 Two-dimensional Thermal Analysis Methodology

The general time-dependent heat equation in 2-D is considered here that includes heat transfer in both *x* and *y* directions (Figure 1) to improve upon solutions from the 1-D heat transfer as modeled in Equation (1). Therefore, a numerical solution instead of a closed-form solution for temperature response is sought using the modified explicit, forward time-centered space finite difference time domain (FDTD) method [1, 11]. Temperatures at an interior point of a finite difference grid is based on a known solution at the grid from the previous iterative step (occurring a time Δt before) as represented in Equation (6).

$$T_{n,m}^{i+1} = T_{n,m}^{i} + \alpha_x \Delta t \frac{T_{n-1,m}^{i} - 2T_{n,m}^{i} + T_{n+1,m}^{i}}{(\Delta x)^2} + \alpha_y \Delta t \frac{T_{n,m-1}^{i} - 2T_{n,m}^{i} + T_{n,m+1}^{i}}{(\Delta y)^2} \tag{6}$$

In Equation (6), α_x and α_y are the thermal diffusivity in *x* and *y* directions (Figure 1), and $T_{n,m}^{i}$ is the temperature at grid point number n (in the *x* direction) and m (in the *y* direction) at timestep i. Unlike other analytical or iterative methods, this explicit method is easily modifiable to incorporate addition of laser energy and changing boundary conditions between different regions.

The 2-D finite difference models the substrate, incoming tape and roller region close to the nip point of the roller where in-situ consolidation takes place. In Figure 3a, all regions are modeled as rectilinear grids, although the roller and incoming tape parts have curvature. However, the region close to the nip point have large radius of curvature and hence has insignificant effect on the thermal response obtained from modeling those parts as rectangular regions of the finite difference grid.

Boundary points are treated as a special-case and have fewer nearest-neighbors than the standard four grid points and use a modification of the difference formula. Additionally, special boundary conditions may apply. For instance, boundaries which represent contact with the aluminum tool plate can be enforced as a constant temperature. The addition of laser energy into the substrate and

incoming tape is treated as a boundary condition as shown in Figure 3a. For this case, laser energy adds heat to the element/grid as heat flux, increasing the temperature.

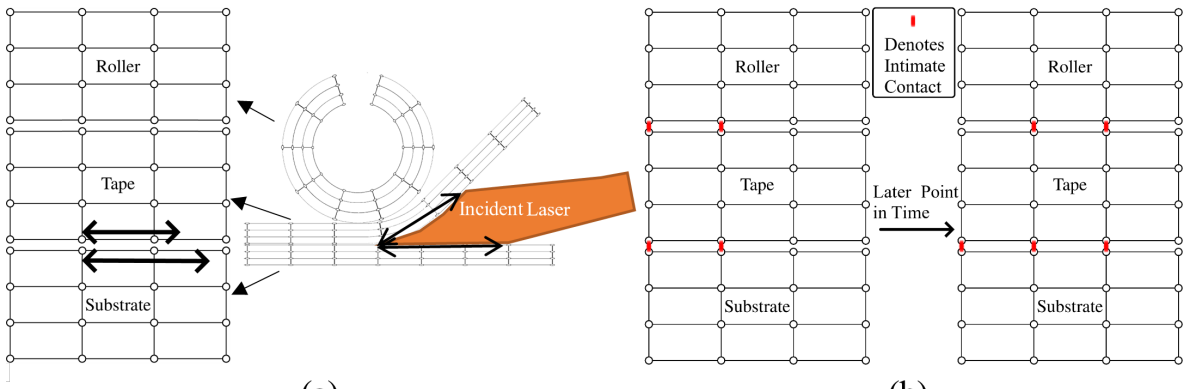

Figure 3: Schematic of 2-D thermal model: (a) incident laser spots and associated regions and (b) thermal contact modeled over time.

Another special boundary condition is the conduction between regions such as incoming tape, substrate, and roller as indicated in Figure 3a. Multiple regions of the assembly are modeled separately and contact conductance between zero and the actual value are applied between regions to represent the extent of contact at any instance of time. This form of thermal contact boundary layer condition is modeled as shown in Figure 3b. Like laser heating, thermal contact changes over time between the different regions. Thermal contact is modeled the same way the rest of the mesh is modeled: by exchange of heat but with the addition of a location-dependent thermal conductivity (or diffusivity) coefficient. Where thermal contact occurs, the thermal conductivity is set to a value similar to that between any other neighboring elements in each region, and care is given to ensure the energy transferred is conserved. Degree of thermal contact can also be changed to account for variable amounts of intimate contact or to compensate for scale. Where thermal contact does not occur, thermal conductivity is set to zero. While the progression of thermal contact was modeled as shown in Figure 3b, the degree of thermal contact between the incoming tape and the roller once in contact were not modeled in great detail. It was assumed that the thermal contact conductance under the roller and after laying down the tape was approximately the same as the bulk thermal conductivity but reduced by 50% for a thickness of about 7 μm (comparable to the surface asperities on the tape).

A more detailed analysis shows that the degree of thermal contact depends on both the pressure applied and the physical properties of the surfaces, such as surface roughness, elastic modulus, and thermal conductivity of the two surfaces. At the microscopic scale, the thermal contact conductance can be approximated by a semi-empirical relationship given by [12]. As the model used laser power as an input (instead of a set maximum temperature limit as in experiment), the model was run multiple times to find the input laser power that would produce the set maximum temperature limit using a simplified version of Newton's Method [11]. In addition to the incident laser energy and the heated tool, there are several other possible methods of changing the temperature of the substrate and incoming tape. Flat-plate convective cooling and radiative cooling were both considered, but their effect was also calculated to be small (on the order of 1-2% each) during the relevant timescales (~2 seconds), so their values are often not used [13].

The basic material properties given in [14] are used in the 2-D simulation as well as in the 1-D simulation. Thermal conductivity along the y direction, specific heat, and density of the thermoplastic tape are 0.34 W/(m·K), 1370 J/(m·K), 1584 kg/m^3, respectively, and 0.2 W/(m·K), 1175 J/(m·K), 1150 kg/m^3, respectively, for the silicon roller. The thermoplastic tape thermal conductivity along the x direction in the 2-D simulation is 3.5 W/(m·K), as in [2]. Several simplifying assumptions were made when modeling these material properties, and representative physical and thermal properties typically found in the literature were used instead of specific measurements of the exact materials used in the ICAT experiments.

The basic features of the 2-D model as typically used are shown in Figure 4. The melt zone is typically smaller than indicated here (this case used an exaggerated power input in order to illustrate the melt zone), however sometimes it does extend another layer deep, remelting the previously laid tape interface. The penetrating heat could potentially give additional time for welding or crystallization to occur. Additionally, the melt zone can extend through the thickness of the incoming tape, causing a risk of the tape welding, or "sticking," to the roller which could peel up the tape as it passes, resulting in the need for repair of the placed surface. The full temperature profile of the composite over time may be difficult or impossible to accurately measure during experimentation, therefore a flexible thermal model such as this is a valuable tool for optimizing the ICAT process. However, it is important to experimentally validate the model as there are several poorly constrained free parameters when developing the model from first principles.

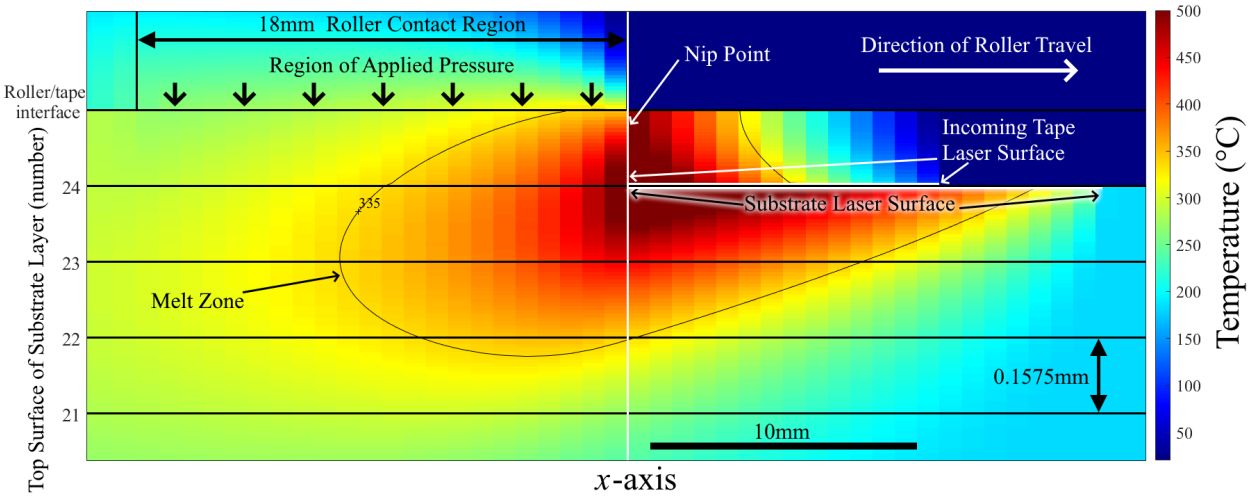

Figure 4: Schematic of the 2-D FDTD thermal model of AFP layup of thermoplastic composites.

3. EXPERIMENTATION

Several ICAT process characterization experiments were conducted [7] at Electroimpact®, Inc. (EI) in their thermoplastic laser-assisted AFP laboratory in Mukilteo, WA. The temperature profile during the ICAT process was measured using a combination of thermocouples and a calibrated forward-looking infrared (FLIR) camera. Commercially available carbon fiber reinforced polyetheretherketone (PEEK) materials were studied in these ICAT process experiments.

3.1 Equipment and Temperature Measurement

The details of the AFP and laser equipment as well as placement of thermocouples and other experimental procedures are published in [1, 7, 15]. In a recent ICAT processing trial [7], the ICAT processing parameters were fixed and the laser angle of incidence (AoI) (θ) was varied from the nominal 16° to 14° and 12° to determine if the resulting increase in laser spot size would result in an increase in the time above the polymer melt temperature. Multiple 24-ply quasi-isotropic panels were fabricated using a layup speed (V) of 25mm/s, a target peak surface temperature (ST) of 525°C, a tool temperature (TT) of 180°C, and Toray® T800/PEEK 6.35-mm wide slit-tape in 3.8-cm wide courses.

During the ICAT processing experiments [7], temperature was measured during layup using a combination of a calibrated forward-looking infrared (FLIR) and thermocouples. The FLIR camera supplied by Teledyne® was mounted on the EI AFP head as indicated in Figure 5, and thermocouples were manually welded to the substrate plies. The data acquired from these two complementary temperature measurement methods were used to plot the temperature profiles presented in this work according to the procedure in [15].

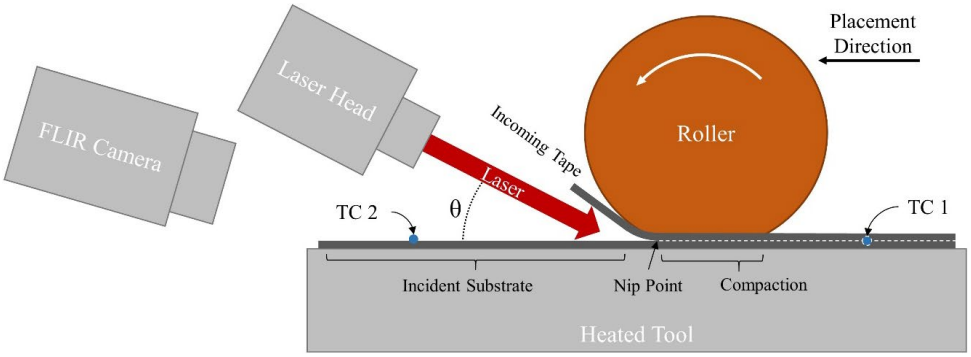

Figure 5: Schematic diagram of laser-assisted AFP.

3.2 Laser Spot Characterization

Measurement of the laser beam AoI and shape was determined using laser alignment paper supplied by ZAP-IT®. Both thermal models assume a rectilinear (and infinitely wide) laser beam of consistent input flux; however, the six spots from the laser beams incident on burn paper (Figure 6a) are elliptical when projected on to the substrate ply and roller and with a varying intensity (due to roller geometry and other effects). The yellow and orange lines represent two possible thermocouple locations, illustrating the uncertainty in effective laser spot size when measured based on thermocouple traces.

An inverted image from the FLIR camera as portrayed in Figure 5 is shown in Figure 6b. The FLIR camera was used during the experimental runs to adjust the laser power to achieve the desired ICAT process target temperature and to evaluate the layup process. This infrared data is also useful for measuring temperature on the incoming tape where it is impractical to measure with thermocouples. This data is, however, limited by uncertainties caused by reflections of infrared

light off the substrate and incoming tape and by uncertainty in the emissivity of the tape which can vary as a function of view angle, and plays a primarily qualitative role in post-experiment analysis.

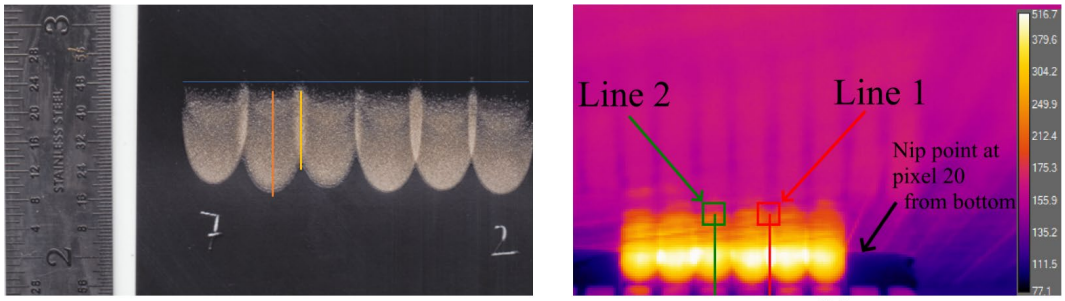

(a) (b)

Figure 6: Laser spot characterization: (a) Laser spot images on laser alignment paper on the roller for the case of an AoI of 12° with equal laser power sent to both incoming tape and substrate (i.e., 50/50) and (b) FLIR image profile locations for an AoI trial of 14° (Color scale is in °C).

4. THERMAL ANALYSIS RESULTS

4.1 One-dimensional Thermal Analysis Results

The objective of the 1-D thermal simulation is to determine the temperature profile of the thermoplastic material at selected manufacturing rates using laser assisted AFP. Multiple 1-D thermal analysis simulations were performed in preparation for the ICAT processing trials. The 1-D thermal simulations were primarily conducted to understand the effects of variation of ICAT parameters, including placement speed, tool temperature, laser AoI, and laser power distribution on the heating response of the thermoplastic tape. The initial 1-D thermal analysis simulation results of earlier ICAT trials with PEEK and LM-PAEK materials are discussed in [1]. To prepare for the ICAT laser AoI trials, the 1-D thermal sensitivity analysis simulations were performed using fixed ICAT parameters for speed, laser target, and heated tool temperature. The laser beam AoIs were varied and were set at 16°, 14°, or 12°. The ICAT AoI study was conducted to understand the effect of laser AoIs on the tape above the melt temperature for extended time in the narrow window of the ICAT consolidation. The 1-D thermal sensitivity analysis included two cases of laser power distribution ratio (50/50 and 40/60) split between the substrate and incoming tape, respectively. The effects of the parameters on the temperature responses shown in Table 1 were determined based on 1-D closed-form formulations. The 1-D thermal analyses of the baseline thermal analysis case 1 having an AoI of 16°, laser power ratio of 50/50, ST of 525°C, TT of 180°C, and V of 25 mm/s resulted in an understanding of the temperature response of the substrate tape.

The temperature responses for the baseline case showing temperature versus placement time are shown in Figure 7. Thermal response curves correspond to temperatures at the substrate top surface, and at various depths from the top surface (quarter, mid-point, and three-quarter of the tape thickness). The substrate tape and the incoming tapes before heating have an initial temperature that correspond to the tool temperature and room temperature, respectively. The heating temperature response curves are parabolic up to the peak temperature. The heat penetration

depth in this semi-infinite substrate model of undefined depth is seen as a function of the square root of the thermal diffusivity and elapsed time. This relationship means that the thermal penetration depth depends on the time of exposure of the material beyond its initial temperature, Equation (2). The incoming and substrate tapes come into contact at the nip-point at two different temperatures and exchange heat, resulting in equilibration. After contact the tapes begin to cool at a very high rate at the nip-point where there is no longer any laser heating. The cooling responses of the substrate and incoming tapes at various tape depths are also plotted in Figure 7a and Figure 7b, which shows a drastic reduction in temperature in less than a second after the loss of laser flux. This drastic cooling effects the time available for polymer molecule reptation and welding [1] as well as crystallization behavior that are critical to the success of in-situ consolidation. The glass transition and melt temperature of the thermoplastic material are indicated in the plots of Figure 7 as horizonal lines for reference to indicate the temperature boundaries for successful in-situ consolidation. The plots also include three vertical lines for reference to indicate the ICAT process time at various points under the compaction roller footprint.

Table 1: 1-D Model results with varying AoI, speed, spot length, and power ratio parameters.

Case	Laser AoI β (°)	Speed V (mm/s)	Substrate Spot h_1' (mm)	Incoming Spot h_2' (mm)	Power Ratio (h_1/h_2)	Power Required (W/m)	Substrate Tape Cooling (Pre-contact)		Incoming Tape Cooling (Pre-contact)		Tape Interface (After contact)
							Max T (°C)	Time Above Melt (s)	Max T (°C)	Time Above Melt (s)	Time Above Melt (s)
1	16	25	11.52	13.80	50 / 50	14.88	525	0.26	336	0	0.04
2	14	25	13.12	11.59	50 / 50	15.86	525	0.32	387	0.01	0.06
3	12	25	15.27	9.37	50 / 50	17.12	525	0.36	461	0.05	0.08

The temperature response of the top surface of the incoming and substrate tape after contact and during consolidation of tapes are plotted in Figure 8a. Consolidation of the heated tapes must occur in the reference time range shown (red to purple timeline). Heating and cooling responses of the tapes for various AoI and power ratio cases are given in Figure 7a and Figure 7b, respectively, as well as time duration above melt temperature, which effects the degree of intimate contact and the consolidation quality. Time above melt increases with reducing angle of incidence as shown in Table 1.

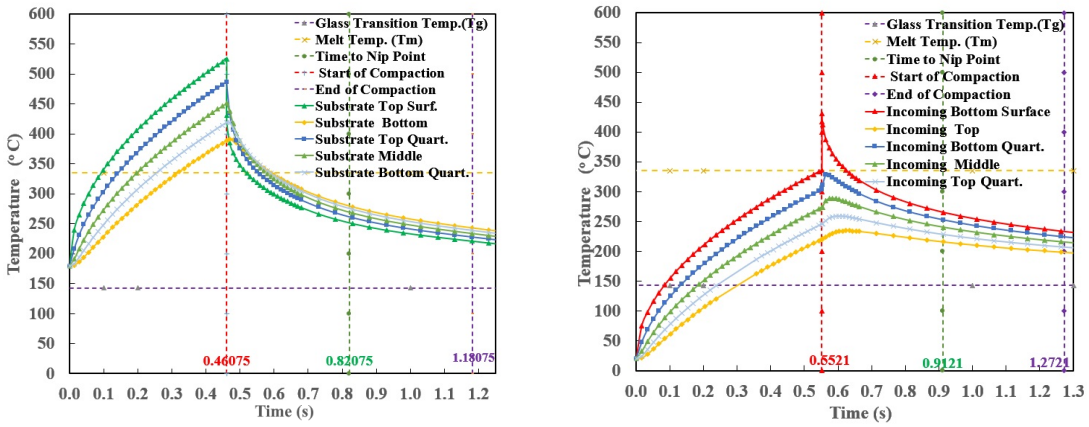

(**a**) (**b**)

Figure 7: 1-D model thermal response of the AoI of 16°, (50/50) case; (a) substrate and (b) incoming tape heating and cooling.

The heating response of the incoming tape calculated using the finite thickness formulation Equation (3) and compared with those of the semi-infinite body are plotted in Figure 8b. There is considerable difference in temperature response between the two. Finite thickness formulation is not included in the analysis here, since the incoming tape is assumed to be in full contact with the roller (Figure 2, case A), where semi-infinite formulation is appropriate.

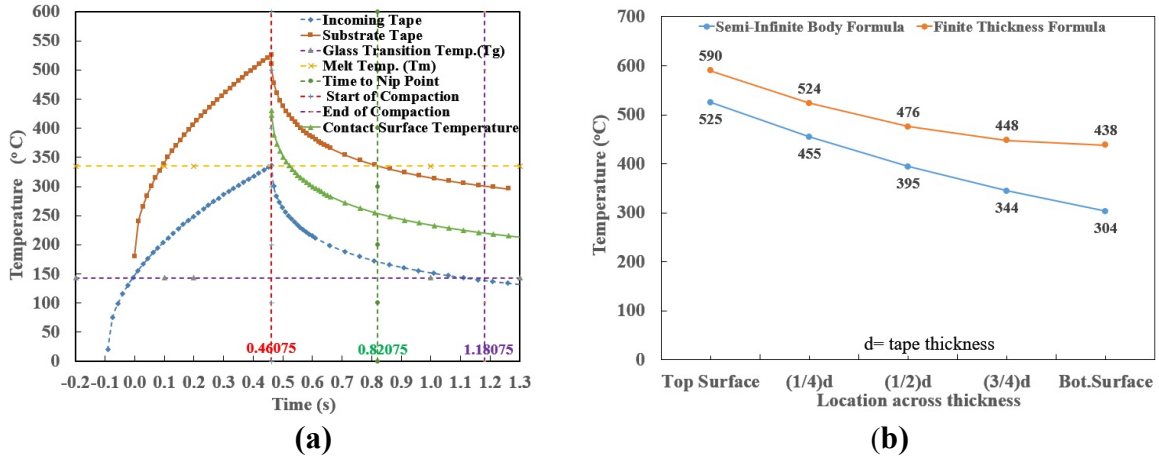

(a) (**b**)

Figure 8: 1-D model results: (a) temperature response before and after contact of top surfaces, and (b) temperature responses from the finite thickness formulation Equation (3) and semi-infinite body formulation Equation (2).

To verify the heating trend from the 1-D thermal analysis predictions with the experimentally measured heating responses of the tape, three cases are considered: (1) AoI of 14°, with power ratio of 50% substrate/50% incoming tape (2) AoI of 14°, with power ratio of 60% substrate/40% incoming tape, and (3) AoI of 12°, with power ratio of 50% substrate/50% incoming tape. All cases had a target peak temperature of 505°C. The thermocouple placement in various layers of the substrate over the heated tool are shown in Figure 9b. The thermocouple measured temperature (TC3) from the experimental data are plotted in Figure 10a, for various AoI. Measured temperature responses follow increasing and decreasing temperature trend similar to what was observed from the 1-D thermal predictions in Figure 9a.

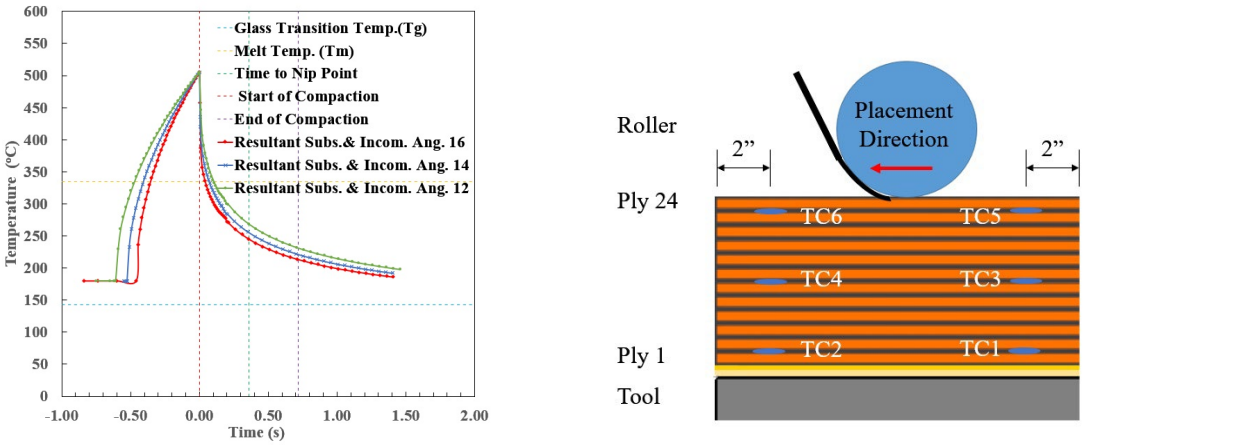

(a) **(b)**

Figure 9: (a) 1-D model sensitivity analysis with respect to AoI and (b) schematic of thermocouple placement.

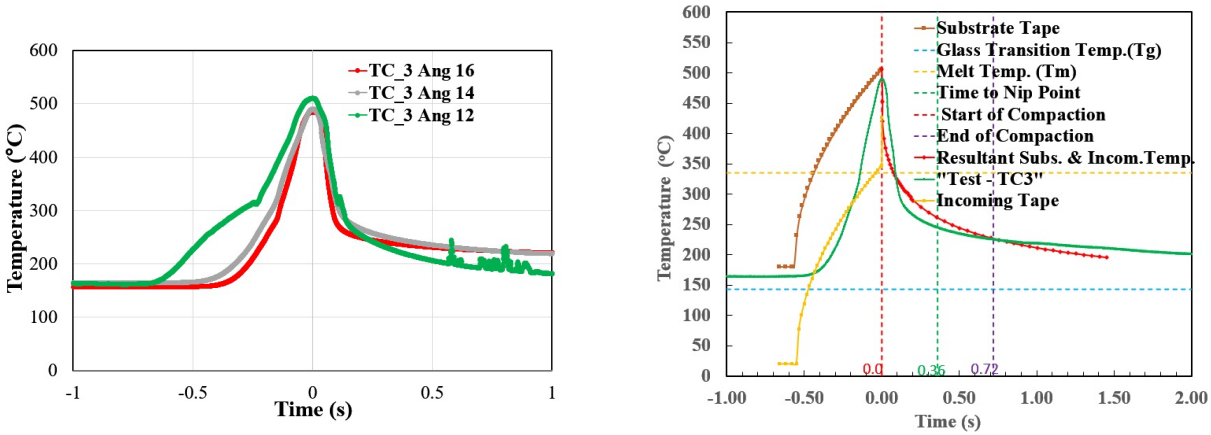

(a) **(b)**

Figure 10: 1-D model comparison: (a) experimental temperatures for three AoI cases and (b) 1-D predictions for the case of AoI of 14° and power ratio of 50/50.

The experimental temperature responses (Figure 10a) for lower AoI have more time above melt similar to those from prediction (Figure 9a), validating the premise that a lower AoI provides heating over a longer period of time in the ICAT process. The 1-D temperature response predictions are compared with experiment data in Figure 10b. For the AoI of 14° with power ratio of 50/50 (Case 1). The initial substrate thermocouple temperatures (TC3) from the experimental data are close to those from the 1-D model prediction, where the incoming tape temperatures are at room temperature. The experimental temperature data in the heating segment increases steadily toward the peak, whereas 1-D predictions are parabolic for reasons noted earlier. In the cooling segment the measured and predicted temperature are similar to the drastic reduction in cooling response (Figure 10b). The results also show the resultant temperatures during the short time segment where tapes come into contact while compacting under the roller nip point. In general, the heating and cooling trends from the 1-D model prediction and experimental data are similar in reaching the peak temperature since target temperature from both the analysis and the experiments are scaled with power.

The cooling trend from both the experimental data and predictions are very similar, indicating that the temperature range attained in the time above melt is accurately predicted. For Case 2 with a power ratio of 60/40 tilted more on the substrate than incoming tape, follows similar trends as in Case 1, but prediction show a longer time of heating with almost no change in cooling response (Figure 11a). The 1-D predictions from Case 3 with AoI of 12° with a power ratio of 50/50 are similar to those predictions for Case 1 and 2. However, the experimental data show differing heating and cooling response (Figure 11b). In the heating segment, a kink is observed in the experimental data, and the cooling segment shows a lower range of measured temperature (with measurement noise) compared to the prediction in the time-temperature window of interest, perhaps indicating that this TC was malfunctioning.

The first order thermal estimates from the 1-D analysis provided peak response and trends comparable to those observed in experimental data acquired during ICAT processing trials. The simplicity of the solution obtained from closed-form formulations represented the essential physics of the thermal problem. Further consideration of features such as varying the heating flux to account for the elliptical shape of the laser spot, and a finite thickness solution for the roller contact will help to improve the predicted trend. The 1-D thermal analysis tool enables an initial estimate of the process temperature required for setting the heating parameters for AFP to evaluate the in-situ consolidation of thermoplastic tapes.

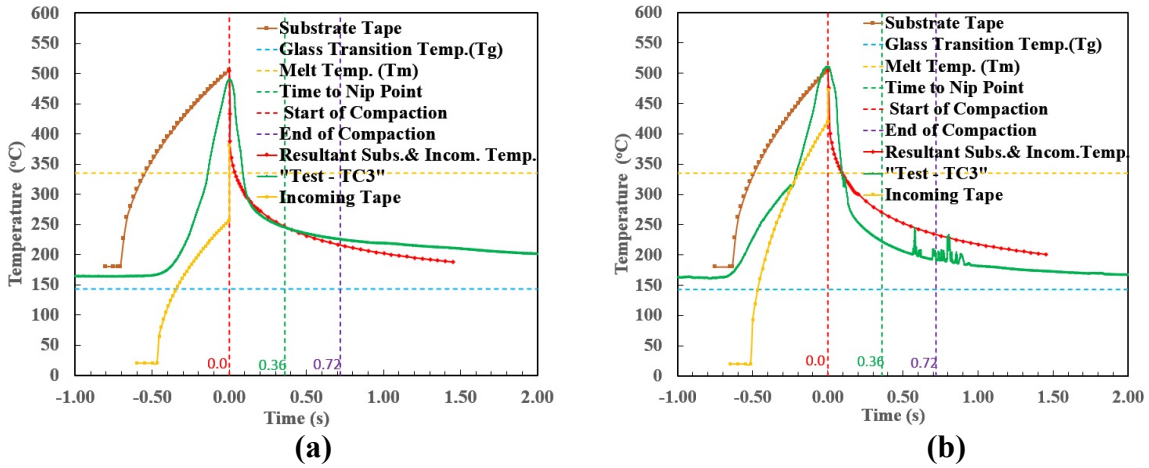

Figure 11: Comparison of temperatures from the 1-D model predictions and TC measurements for the case of (a) AoI of 14°, power ratio of 60/40 and (b) AoI of 12°, power ratio of 50/50.

4.2 Two-dimensional Thermal Model Results

The 2-D thermal modeling of the layup process was used to predict the time the material is above the crystalline melt temperature of 335°C for PEEK and its temperature profile while under compaction pressure. The coding and solution of the finite difference algorithms in MATLAB® provides a flexible method to investigate and understand anomalies found in temperature measurements during the ICAT experiments. Simulations were run for the following three cases labeled by panel according to the experimental notation (with Panels 2 and 4 corresponding to the 1-D model cases in Table 1, Case 2 and 3) from the laser AoI ICAT experiments [7]:

- 14° AoI, Power - 50% substrate/50% incoming tape (Panel 2)
- 14° AoI, Power - 60% substrate/40% incoming tape (Panel 3)
- 12° AoI, Power - 50% substrate/50% incoming tape (Panel 4)

The 2-D simulations for Panel 3 resulted in the substrate and incoming tape at the most similar temperature when joined, matching the experimental data except that the laser exposure time modeled for the substrate (based on the laser alignment paper data) was somewhat longer than the thermocouple data indicated as shown in Figure 12a through Figure 12c. This discrepancy may be due to the elliptical geometry of the laser spot. The thermocouple bead may have also been located in the trough of the laser ellipses where the spots overlap slightly, indicated by the yellow line in the FLIR image in Figure 6a or Line 1 in Figure 6b. Panel 2 had exposure times with a slightly smaller discrepancy than Panel 3. Panel 4 had laser exposure times similar between that measured by the alignment paper and that indicated by the TC3 thermocouple. These times indicate the thermocouple sensor may have been in a position similar to the orange line in the FLIR image in Figure 6a or Line 2 in Figure 6b.

The initial 1-D and 2-D simulations (as in Figure 12d) had been conducted under the assumption of high thermal contact between the incoming tape due to the tension of the tape against the roller ahead of the nip point, which would cause heat incident on the incoming tape to be transferred into

the roller. However, the temperature measured during the experiments indicated that the incoming tape was heating higher than expected. Therefore, the true thermal contact with the roller ahead of the nip point was reevaluated, and analysis using no pre-nip thermal contact between the roller and incoming tape was conducted, showing qualitatively better agreement with the experimental data (Figure 12a through Figure 12c). For instance, in the simulation for Panel 2 that assumed pre-nip-point roller thermal contact (Figure 12d and Figure 13a), the incoming tape was lower in temperature than the substrate before the nip point which contradicts the experimental observations of the FLIR imaging, which showed the incoming tape to have a higher temperature than the substrate. Modeling the roller to be insulating until the nip point (Figure 12a and Figure 13b) shows the same trend as the experiment (Figure 14), which better matches temperature profiles measured along the lines in Figure 6b.

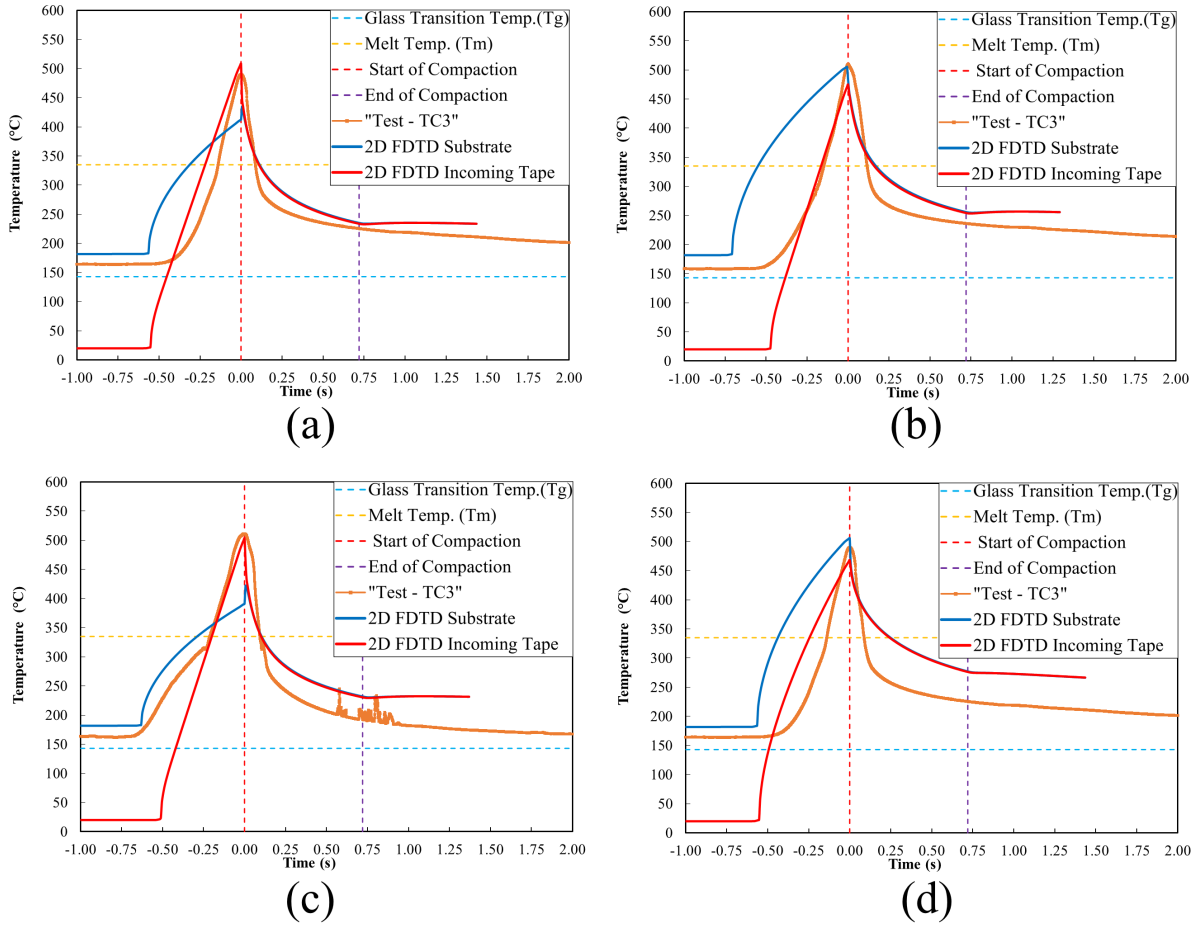

Figure 12: 2-D modeling results (with no pre-nip-point thermal contact) of (a) Panel 2, (b) Panel 3, (c) Panel 4, and (d) Panel 2 assuming pre-nip-point roller thermal contact with the incoming tape.

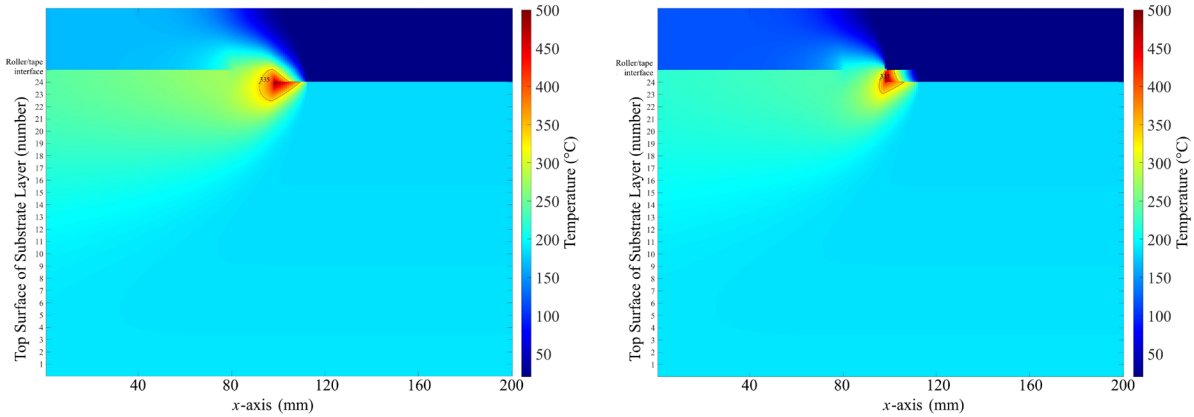

Figure 13: 2-D modeling results: (a) with pre-nip-point thermal contact and (b) without pre-nip-point thermal contact.

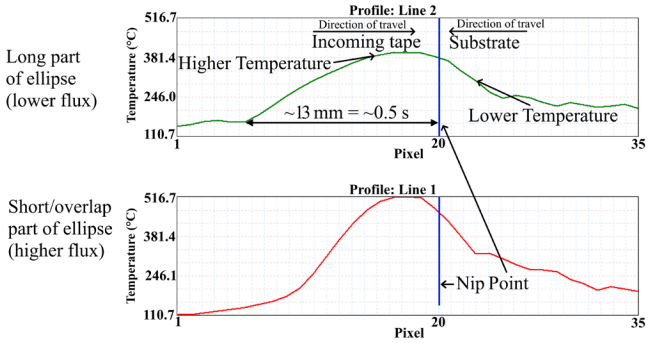

Figure 14: Thermal infrared temperature profiles (not to linear scale) for Panel 2.

Table 2: Analysis results of the 2-D FTDT model.

Panel	Pre-nip Roller/Tape Thermal Contact?	β (°)	Substrate Spot h_1' (mm)	Incoming Arc h_2' (mm)	Power Distribution (h_1/ h_2)	Power (W/mm²)	Pre-nip Max. Temperature Target (°C)	Under Compression Time Above Melt (s)	TC3 Post-peak Time Above Melt (s)	Ratio of Experimental Time Above Melt to Simulation
2	No	14	14.14	13.81	46 / 54	7.208	505	0.1122	0.0875	80%
3	No	14	17.68	11.78	60 / 40	8.801	505	0.17082	0.1160	68%
4	No	12	15.90	12.90	46 / 54	7.042	505	0.0986	0.0930	94%
2	Yes	14	14.14	13.81	46 / 54	10.218	505	0.2479	0.0875	35%
3	Yes	14	17.68	11.78	60 / 40	8.8571	505	0.08972	0.1160	129%
4	Yes	12	15.90	12.90	46 / 54	10.663	505	0.2922	0.0930	32%

Assuming a lower pre-nip-point thermal contact in the 2-D model, the time above melt after the nip-point more closely matches the experimental data (Table 2) when comparing the two simulation runs for Panel 2. Assuming thermal contact ahead of the nip-point over-estimates the time above melt (under compression) by nearly a factor of 3 (experimental time above melt of 0.0875 s vs 2-D model time above melt of 0.2479 s), but assuming no pre-nip thermal contact

agrees with experiment to within 20% (experimental time above melt of 0.0875 s vs modeled time above melt of 0.1122 s).

The objective of the ICAT AoI experiments [7] was to determine if reducing the laser AoI (thereby increasing the spot length on the substrate ply) would increase both the time above melt as well as weld strength. Comparing Panel 2 and 4, corresponding to 14° and 12° AoI, respectively, with the same power ratio in Table 2 for the no pre-nip thermal contact case shows that reducing the incident angle does not improve the time above melt in the model (reduces from 0.1122 s to 0.0986 s) and only marginally improves time above melt experimentally (from 0.0875 s to 0.0930 s). The lack of improvement in the model results is because the incoming tape already reaches the temperature limit as shown in Figure 12a and Figure 12c. These results indicate that reducing the AoI reduces the distance and, thereby, the time for heat to transfer before the ST limit is reached for the laser spot on the incoming tape. The reduced heat transfer time causes the modeled temperatures to be lower on the substrate (than the incoming tape) when the nip point is reached. In contrast, with assumption of pre-nip-point thermal contact (Figure 12d), the modeled temperature is higher on the substrate (than the incoming tape). The time above melt under compression was expected to increase (from 0.2479 s to 0.2922 s) with decreasing laser AoI (from 14° to 12°) using the assumption of pre-nip-point thermal contact as shown in Table 2.

During the ICAT AoI processing trial [7], the effect of changing the ratio of laser power between the substrate and the incoming tape was also investigated for the three AoIs. Under the high pre-nip-point thermal contact assumption, simulations showed that for the 14° AoI reducing the power ratio (from 60/40 to 46/54) to provide proportionally more power to the incoming tape would increase the time above melt (from 0.08972 s to 0.2479 s) because the cold roller would absorb more heat from the incoming tape before the nip point. In fact, the opposite was observed in the experiment data. Panels 2 and 3 had the same angle, but the lower laser ratio for Panel 2 reduced the time above melt compared to Panel 3 (from 0.1160 s to 0.0875 s). The simulation results using the no pre-nip-point thermal contact assumption (Table 2) have a reduced time above melt (from 0.17082 s to 0.1122 s) for the reduced power ratio (from 60/40 to 46/54), consistent with the experimental trend.

5. SUMMARY AND CONCLUSIONS

1-D and 2-D thermal modeling tools were successfully developed to perform analysis of the ICAT process, enabling a more thorough understanding of the processing constraints. These tools were validated against experimental data and used to help guide the experimental procedures. The analytical 1-D thermal model enabled a quick, first look approximation which was useful for trading basic quality versus speed choices. A more flexible 2-D FDTD model was used to further explore the constraints of the process and learn which process variables provide the best opportunity to enhance out-of-autoclave thermoplastic composite fabrication. The ICAT processing experiments [7] were designed based on insights gained from the models; and the immediate results of these experiments yielded valuable information to reevaluate the models, including the degree of thermal contact and heat transfer between the incoming tape and the AFP compaction roller. With this experiment-informed approach, the 2-D FDTD model was enhanced with more realistic assumptions. The revised model was further validated by the experimental results [7] which largely agreed with the new predicted trends in the tape time above melt, as indicated by the measurement of the tape temperature immediately before the nip point. The

success of the model development is tempered by the fact that many of the inputs used in the models are still poorly constrained at this point. The characterization of the thermo-physical properties of PAEK tapes is ongoing at NASA to verify the values obtained from the literature and currently used in the models. The models developed in this work provide a strong basis for further development.

6. REFERENCES

[1] B. W. Grimsley, R. J. Cano, T. B. Hudson, F. L. Palmieri, C. J. Wohl, R. I. Ledesma, T. Sreekantamurthy, C. J. Stelter, M. D. Assadi, R. F. Jordan, J. H. Rower, R. A. Edahl, J. C. Shiflett and J. W, "In-Situ Consolidation Automated Fiber Placement of Thermoplastic Composites for High-Rate Aircraft Manufacturing," in *SAMPE 2022*, 2022. doi:10.33599/nasampe/s.22.0870.

[2] J. Tierney and J. W. Gillespie, "Modeling of In Situ Strength Development for the Thermoplastic Composite Tow Placement Process," *Journal of Composite Materials,* vol. 40, no. 16, pp. 1487-1506, January 2006. doi:10.1177/0021998306060162.

[3] S. M. Grove, "Thermal modelling of tape laying with continuous carbon fibre-reinforced thermoplastic," *Composites,* vol. 19, no. 5, p. 367–375, September 1988. doi:10.1016/0010-4361(88)90124-3.

[4] M. D. Francesco, L. Veldenz, G. Dell'Anno and K. Potter, "Heater power control for multi-material, variable speed Automated Fibre Placement," *Composites Part A: Applied Science and Manufacturing,* vol. 101, pp. 408-421, October 2017. doi:10.1016/j.compositesa.2017.06.015.

[5] C. M. Stokes-Griffin and P. Compston, "A combined optical-thermal model for near-infrared laser heating of thermoplastic composites in an automated tape placement process," *Composites Part A: Applied Science and Manufacturing,* vol. 75, pp. 104-115, August 2015. doi:10.1016/j.compositesa.2014.08.006.

[6] T. Weiler, M. Emonts, L. Wollenburg and H. Janssen, "Transient thermal analysis of laser-assisted thermoplastic tape placement at high process speeds by use of analytical solutions," *Journal of Thermoplastic Composite Materials,* vol. 31, no. 3, pp. 311-338, March 2017. doi:10.1177/0892705717697780.

[7] B. Grimsley, T. Hudson, R. Cano, J. Shiflett, C. Stelter, C. Wohl, R. Ledesma, T. Sreekantamurthy, J. Kang, J. Nancarrow, R. Jordan and J. Rower, "Laser Angle of Incidence Effects on In-situ Consolidation Automated Fiber Placement of Thermoplastics," in *SAMPE Conference*, May 2024 (in-press).

[8] A. Bejan and A. D. Kraus, Eds., Heat transfer handbook, vol. 1, John Wiley & Sons, 2003.

[9] F. Amir, Y. Zhang and J. R. Howell, Advanced heat and mass transfer, Global Digital Press, 2010, ISBN: 0984276009.

[10] F. P. Incropera, Fundamentals of heat and mass transfer, vol. 6, New York: Wiley, 2006.

[11] E. H. Smith, Ed., Mechanical engineer's reference book, 12th ed., Butterworth, 1994.

[12] J. J. Fuller and E. E. Marotta, "Thermal Contact Conductance of Metal/Polymer Joints: An Analytical and Experimental Investigation," *Journal of Thermophysics and Heat Transfer,* vol. 15, no. 2, pp. 228-238, April 2001. doi:10.2514/2.6598.

[13] Mayahtt.com, "Convection Wizard," [Online]. Available: https://thermal.mayahtt.com/tmwiz/convect/natural/hup-isot/hup-isot.htm. [Accessed 15 December 2023].

[14] J. Tierney and J. W. Gillespie, "Modeling of Heat Transfer and Void Dynamics for the Thermoplastic Composite Tow-Placement Process," *Journal of Composite Materials,* vol. 37, no. 19, pp. 1745-1768, October 2003. doi:10.1177/002199803035188.

[15] T. B. Hudson, C. T. Dolph, G. M. Grose, R. J. Cano, R. F. Jordan, C. J. Wohl, R. I. Ledesma and B. W. Grimsley, "Thermal Response of Thermoplastic Composite Tape During In-situ Consolidation Automated Fiber Placement Using a Laser Heat Source," in *SAMPE 2023*, 2023. doi:10.33599/nasampe/s.23.0101.